Inteferometry on a single aperture

OUTLINE:

Why interferometry on a single aperture ?
advantage of interferometric techniques on single aperture telescopes: high precision measurements enabled by good calibration

Aperture masking
(slides adapted from presentation by Frantz Martinache)

Pupil remapping

Interferometry as a technique to analyze single aperture short exposures:
Speckle interferometry

Interferometry on a single aperture: First Aperture Masking experiment

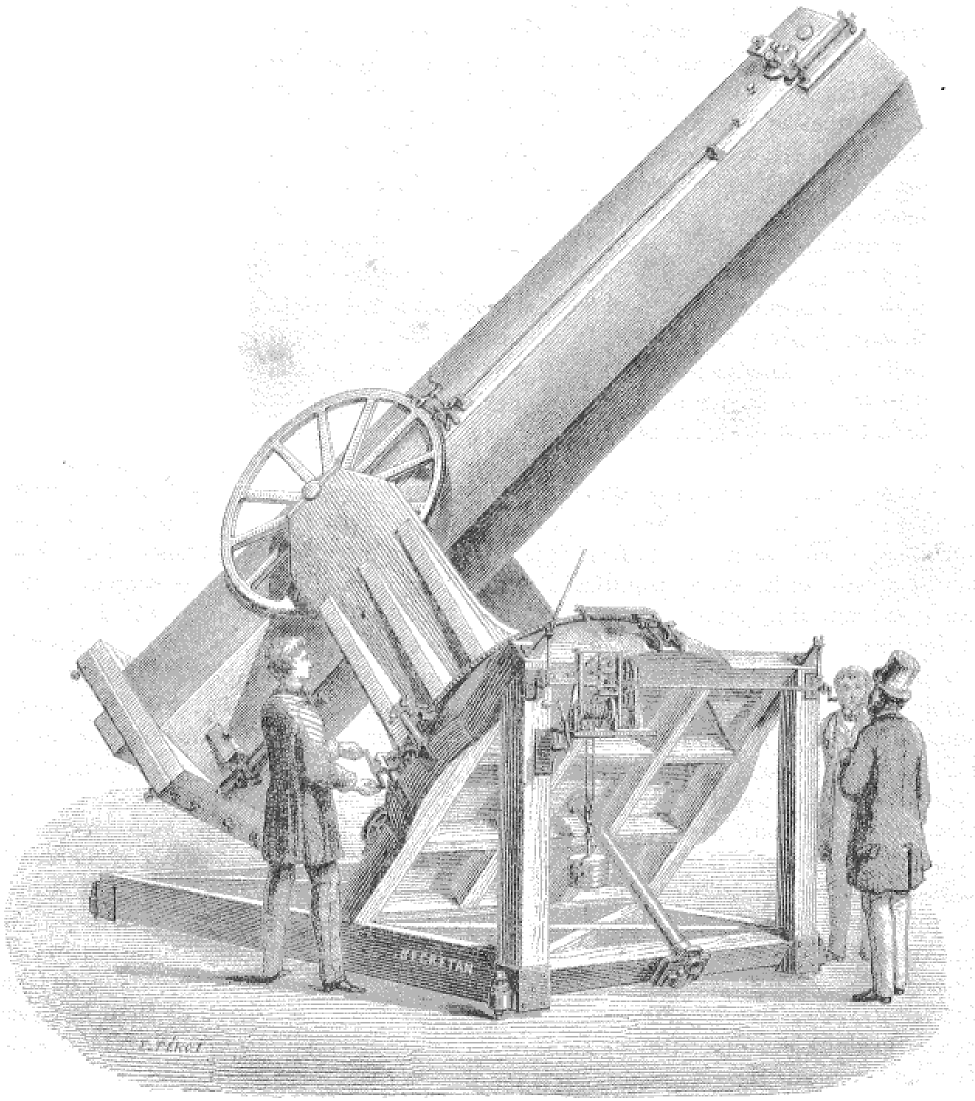

Le grand télescope Foucault, de l'Observatoire de Marseille.

Marseille 1873, *Edouard Stephan attempts at measuring the diameter of stars.*

Baseline of 80 cm,
$\varnothing_{\star} < 0.16''$

Michelson later improved the experiment with an beam expanding the baseline, and was the first to resolve stars

Aperture masking: principle

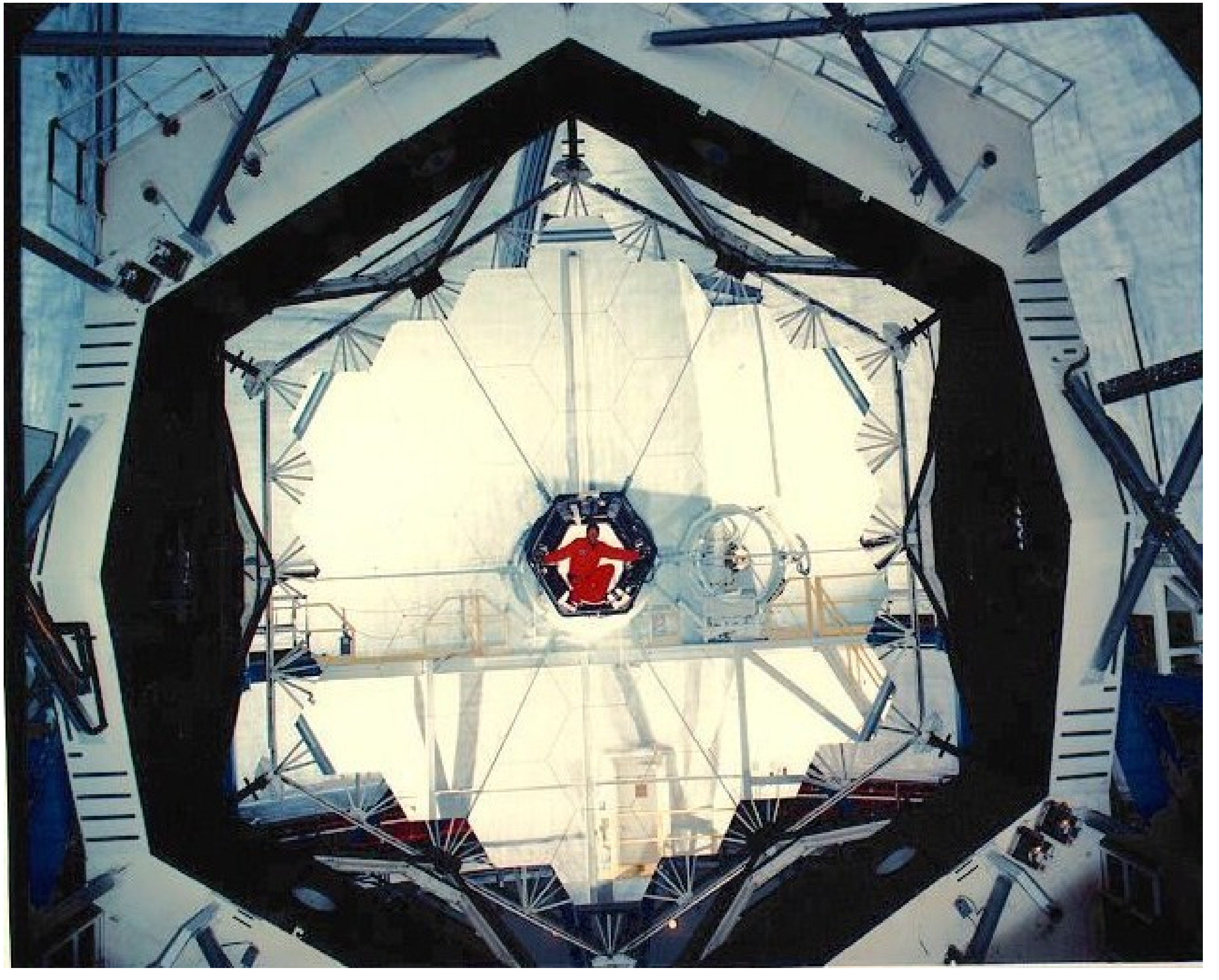

Aperture masking: principle

ref: *Tuthill et al, 2000, PASP, 112, 555*

Fizeau Interferometry

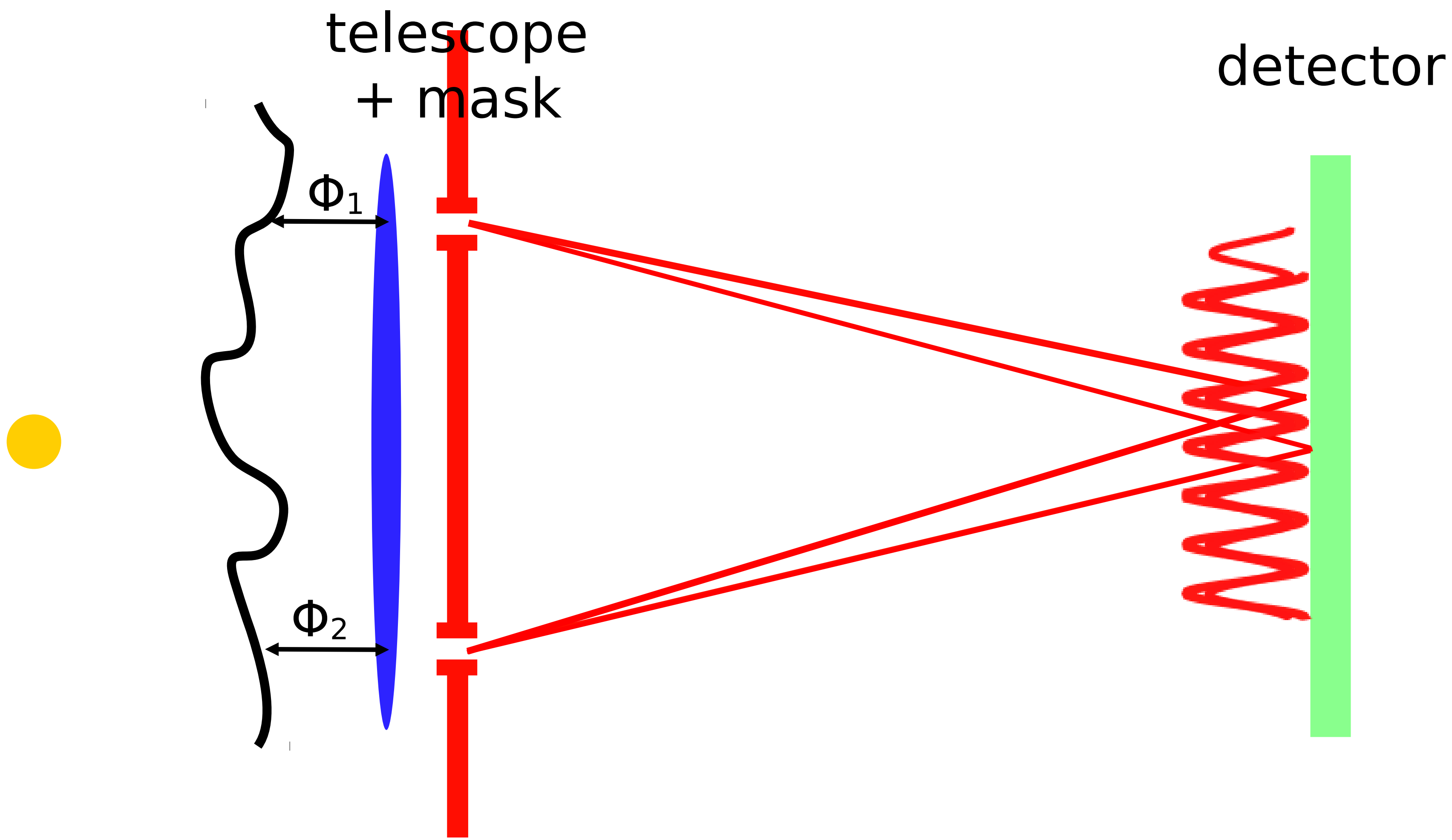

visibility:

$0 < V^2 < 1$

phase:

$\Phi = \Phi_0 + (\Phi_1\text{-}\Phi_2)$

Redundancy: **Atmosphere affects the phases, Redundancy destroys the amplitudes**

Redundant

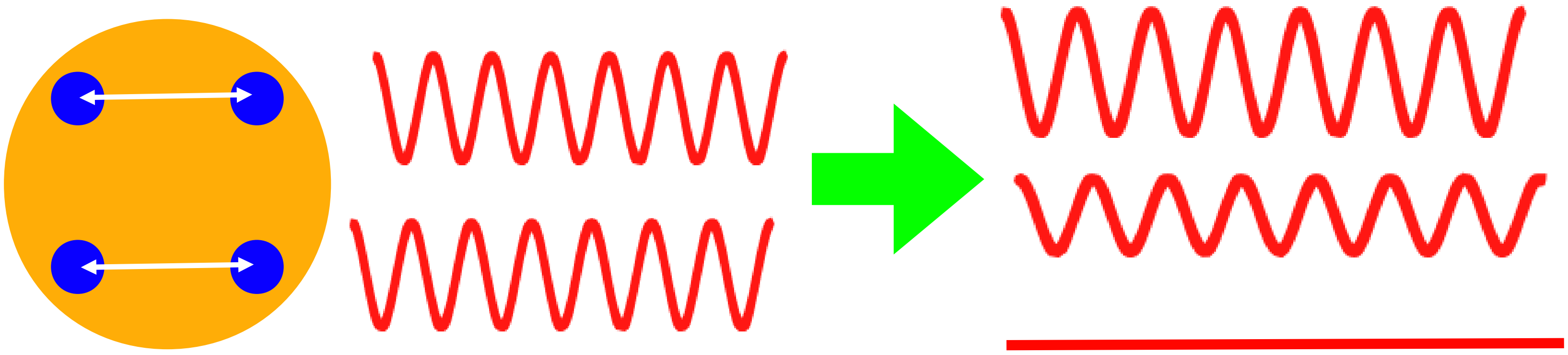

fringe amplitude is function of phase offset between baselines
→ **visibilities and phases cannot be measured**

Non Redundant

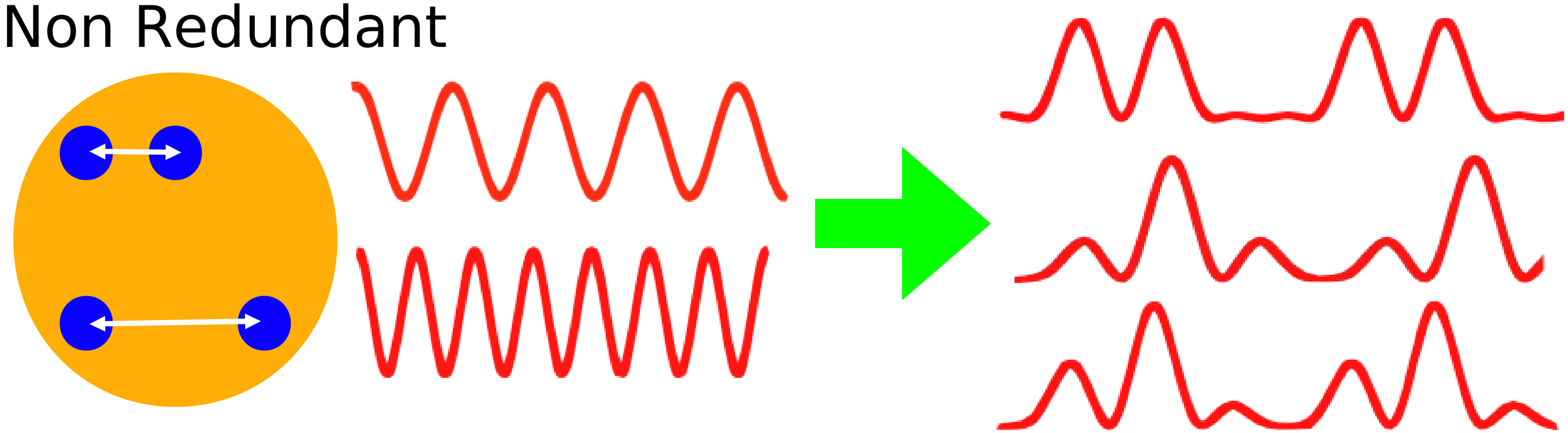

different baselines at different frequencies
→ **visibilities and phases can be isolated by Fourier Transform**

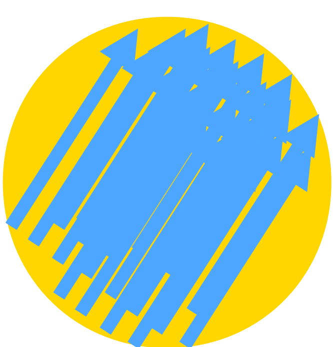

A full aperture is very redundant

Aperture Masking: creating non-redundant aperture with pupil mask

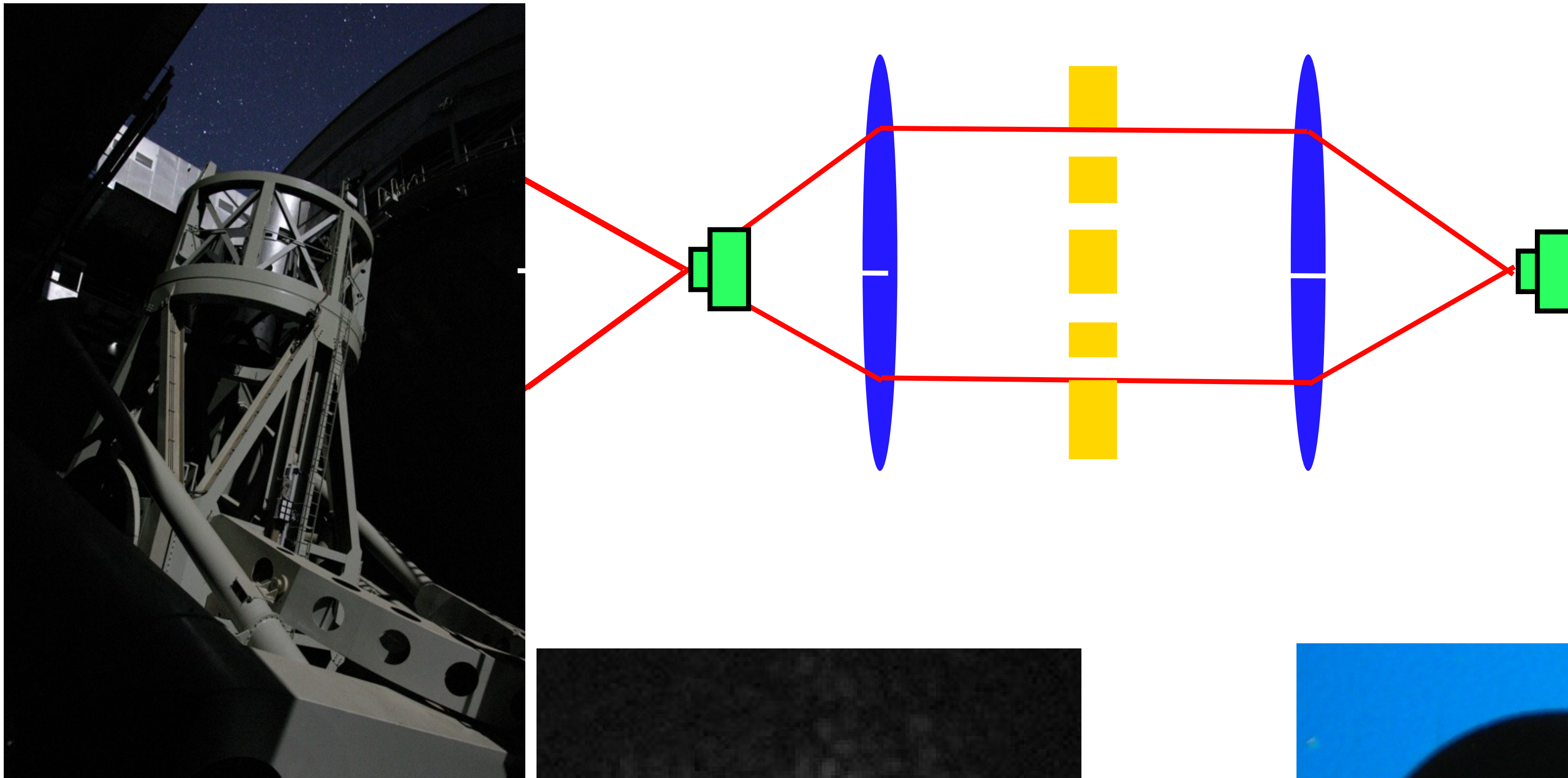

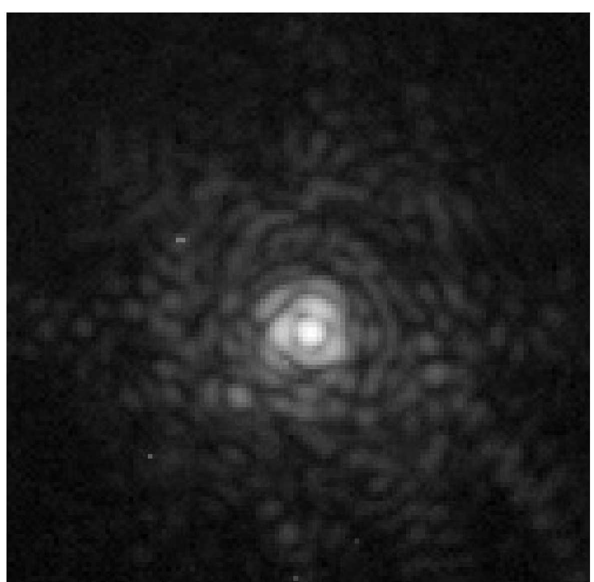

Image and Fourier planes

conventional imaging

aperture masking

Image

$|FT|^2$

Modulation Transfer Function

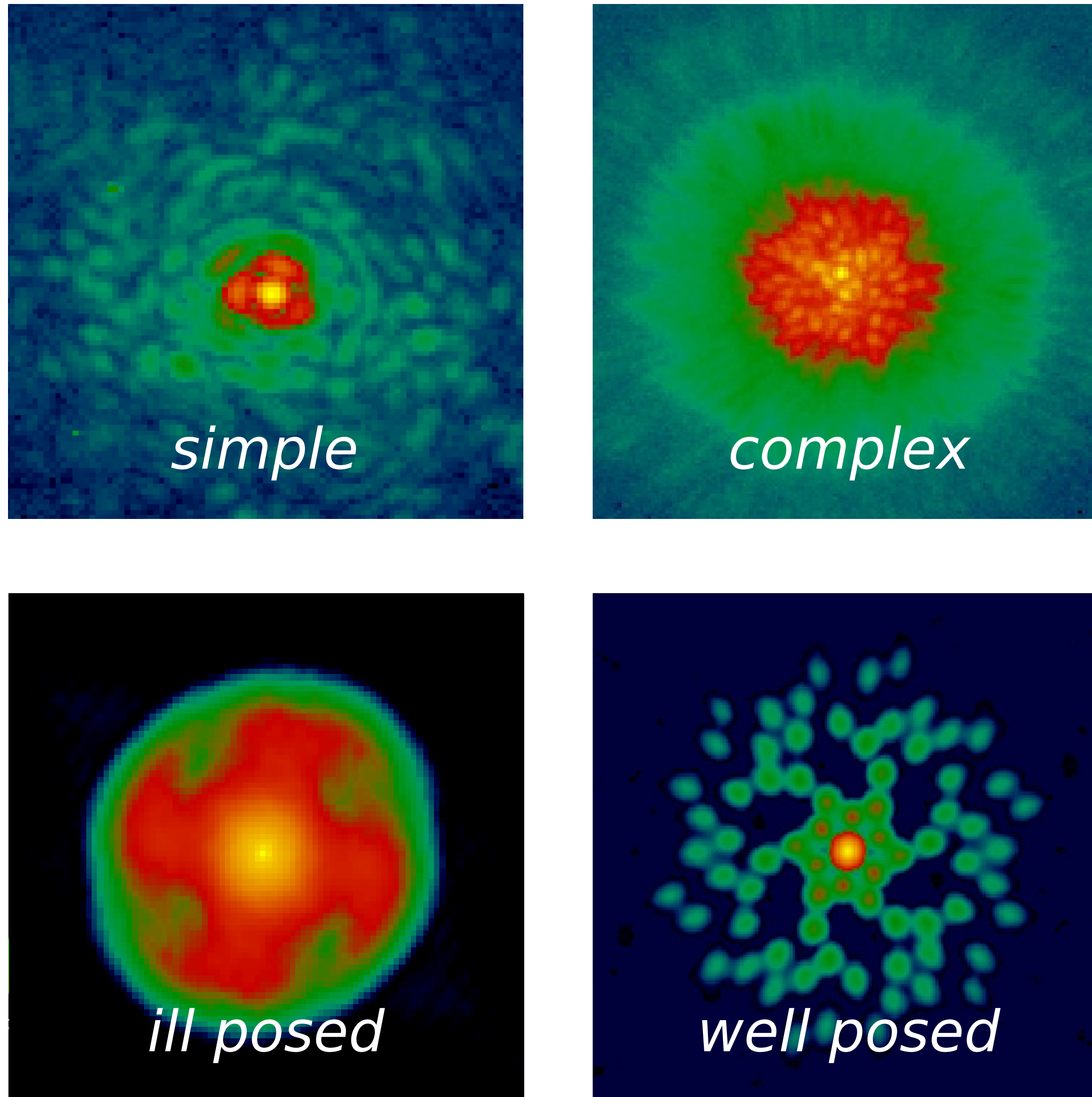

A neat trick: the closure phase

9-hole mask
36 visibilities
84 triangles
(28 independent)

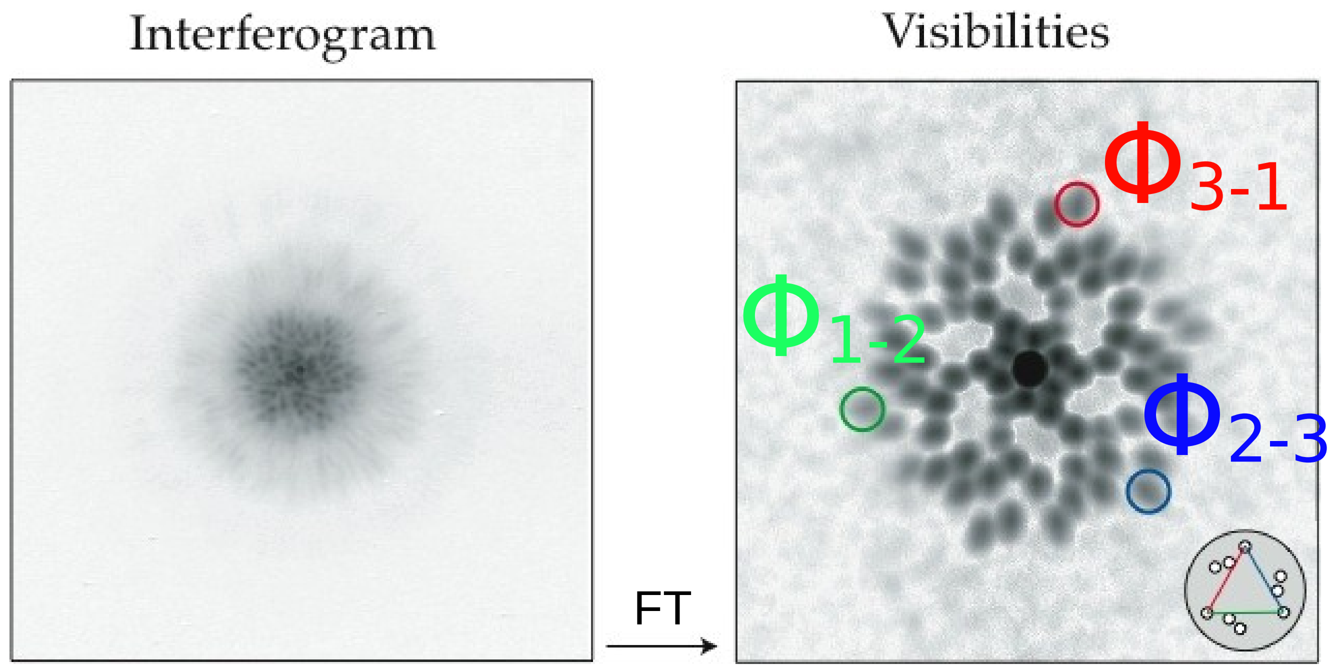

$\Phi(1\text{-}2) = \Phi(1\text{-}2)_0 + (\Phi_1\text{-}\Phi_2)$

$\Phi(2\text{-}3) = \Phi(2\text{-}3)_0 + (\Phi_2\text{-}\Phi_3)$

$\Phi(3\text{-}1) = \Phi(3\text{-}1)_0 + (\Phi_3\text{-}\Phi_1)$

measured = intrinsic + atmospheric

Closure phases are invariant to atmospheric phase

cancels out in closure phase sum

Binary systems

3 parameters: angular separation, position angle, contrast
Error estimate: closure phase scattering
Small systematic error

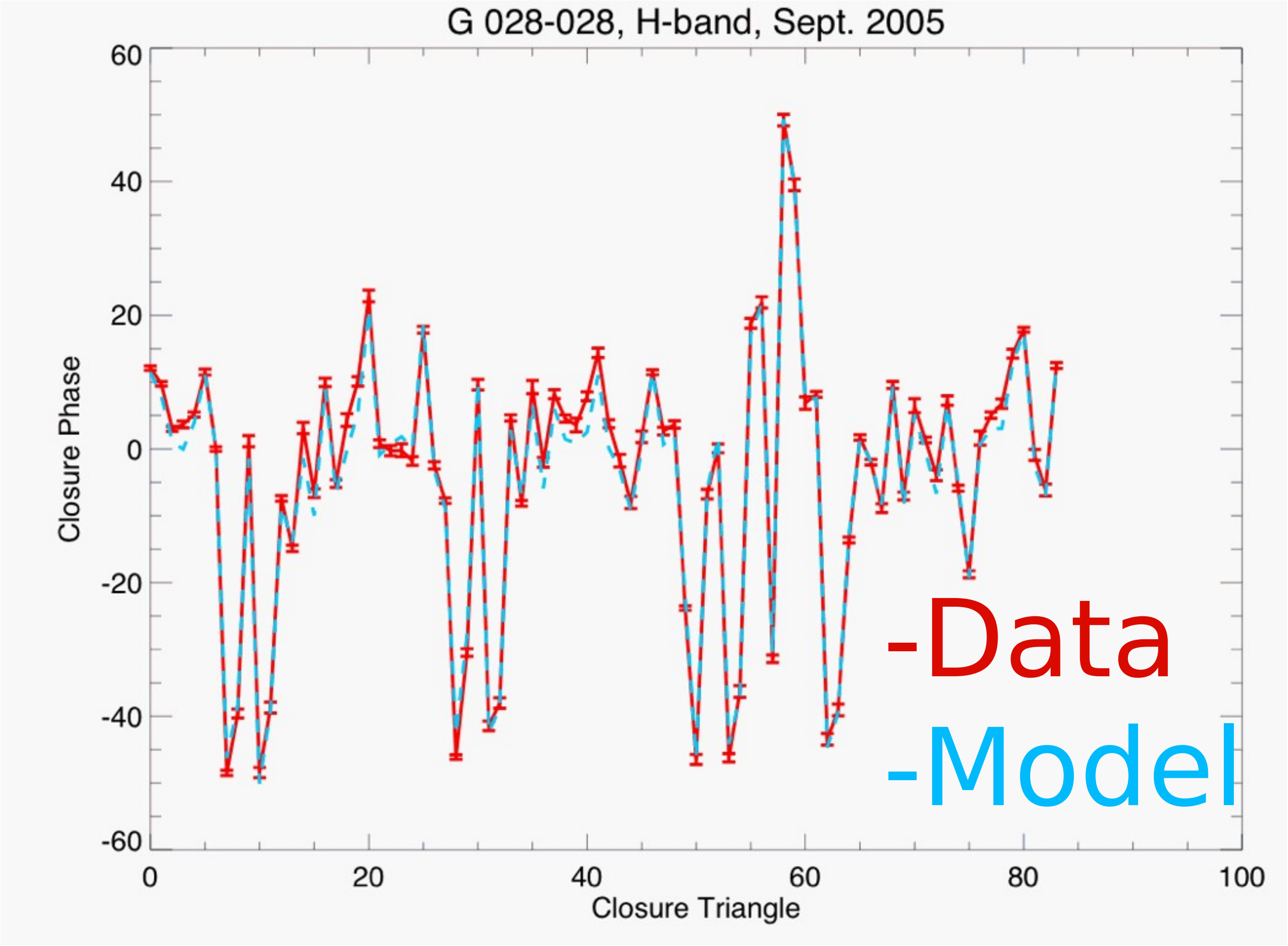

40 % strehl
0.3 deg scatter
stability ~ λ/1000
all passive !

An example of super-resolution

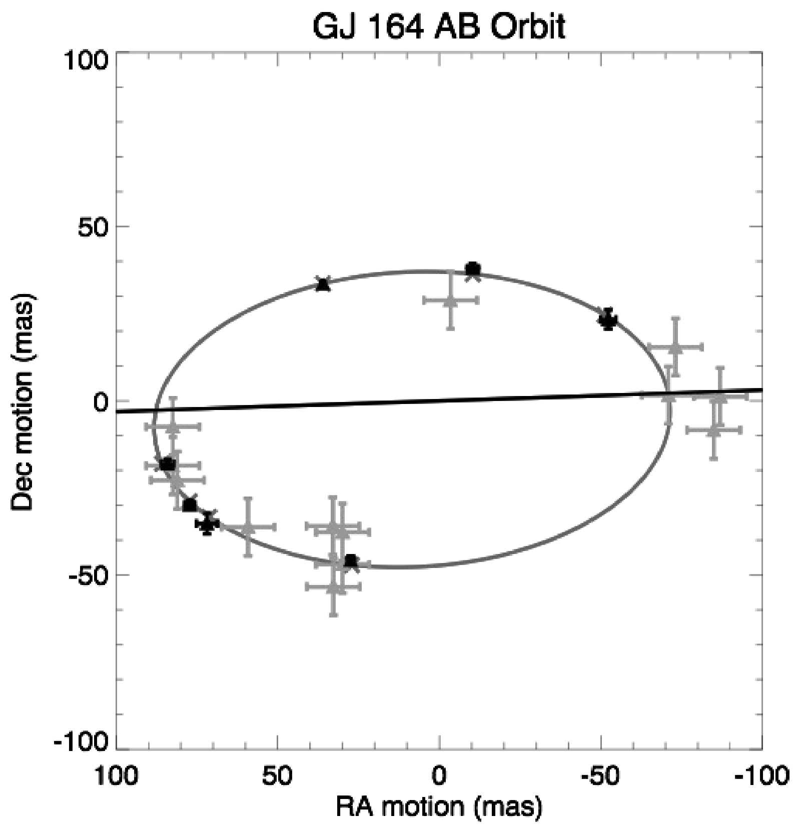

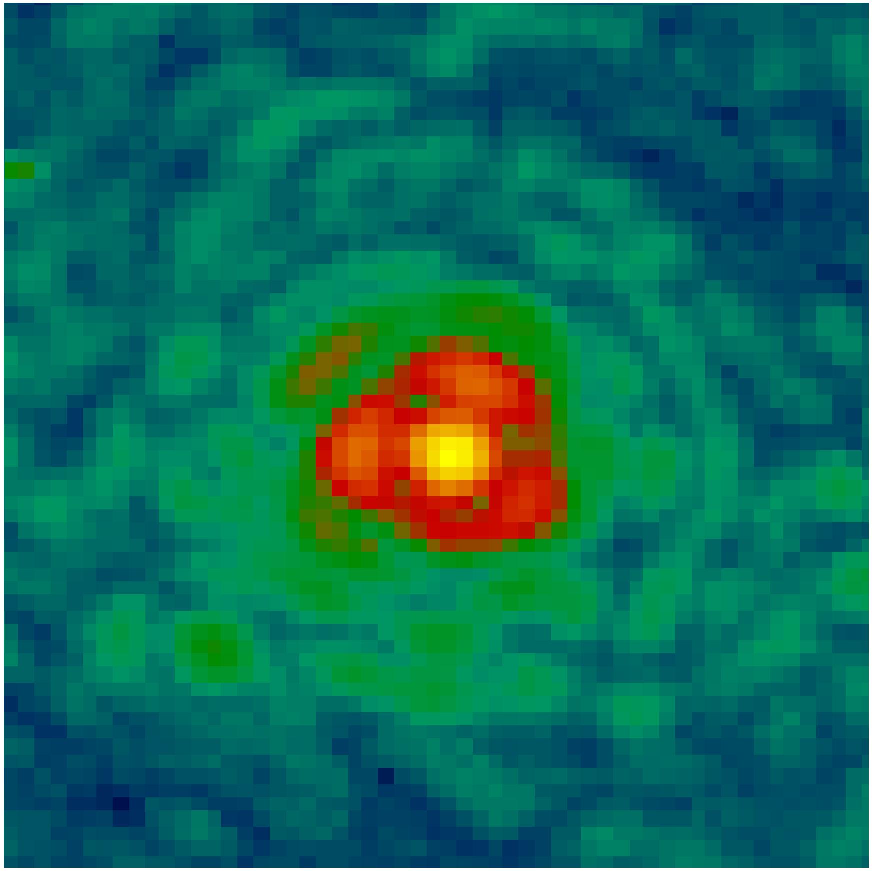

Black points: masking measurements
Grey points: STEPS astrometry

H-band image of GJ164 by the Hale Telescope

$\lambda/D = 66$ mas

Example result

LkCa 15: A Young Exoplanet Caught at Formation? (Kraus & Ireland 2012)

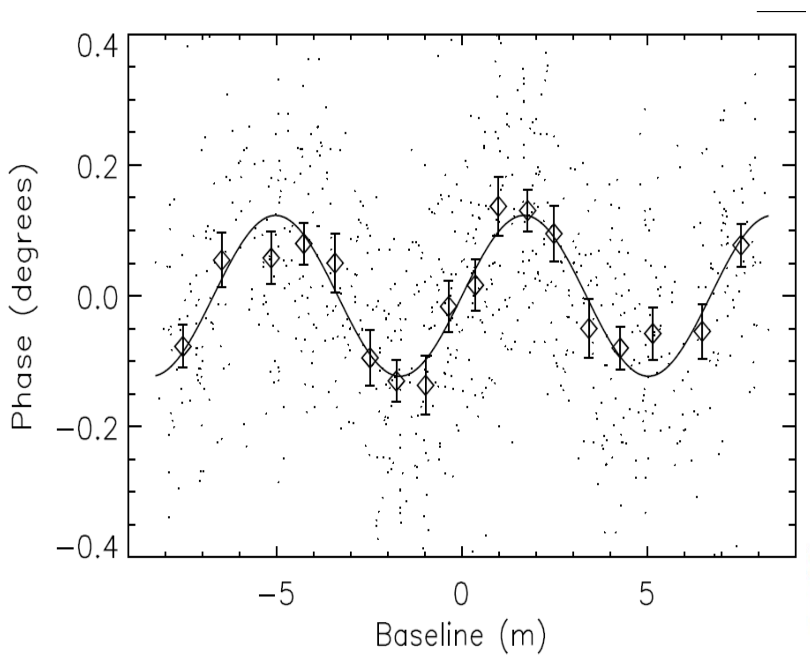

FIG. 1.— Fourier phase fitted to closure-phase (small dots) and the binned version of the same observable (triangles) for all 2010 K-band data on LkCa 15, plotted against the baseline projected along the principle axis of the best fit binary model. The phases of the best fit binary model model from Table 2 is shown as a solid line..

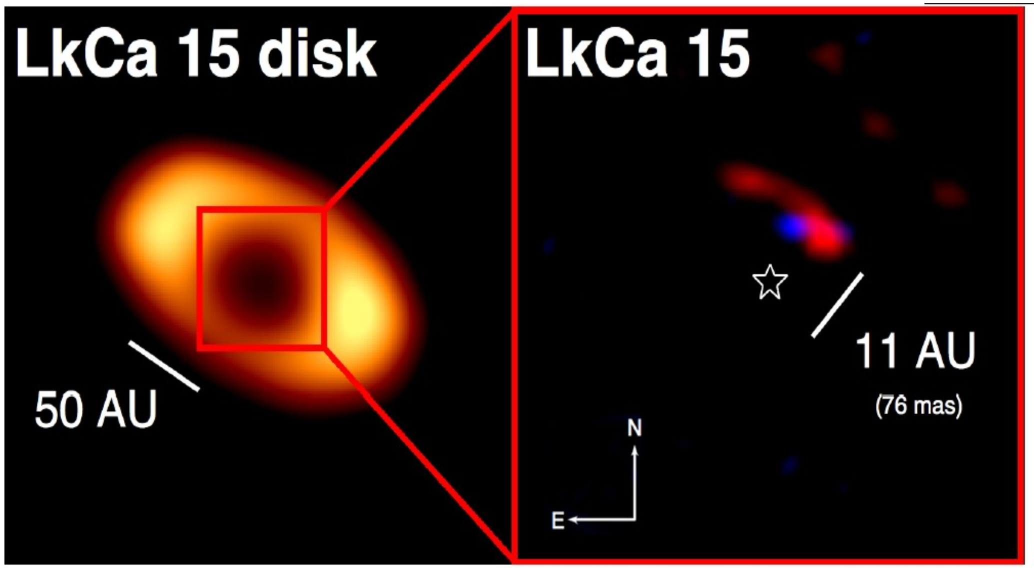

FIG. 3.— Left: The transitional disk around LkCa15, as seen at a wavelength of 850 μm (Andrews et al. 2011). All of the flux at t wavelength is emitted by cold dust in the disk; the deficit in the center denotes an inner gap with radius of $\sim$55 AU. Right: An expand view of the central part of the cleared region, showing a composite of two reconstructed images (blue: K' or $\lambda = 2.1$ μm, from Novemb 2010; red: L' or $\lambda = 3.7$ μm, from all epochs) for LkCa 15. The location of the central star is also marked. Most of the L' flux appears come from two peaks that flank a central K' peak, so we model the system as a central star and three faint point sources.

Closure phases + fit for binary model

Reconstructed image (right)

Beyond conventional aperture masking

Aperture masking offers high degree of calibration (= high precision) but is not very efficient (only a small fraction of the light is preserved). (u,v) coverage is limited by non-redundancy:

- large holes = high throughput, but fewer holes to avoid redundancy
- small holes = many holes, but small throughput

→ **Aperture masking is most suitable for simple (compact) and bright objects**

In aperture masking, non-redundancy needs to be imposed at the detector, not at the entrance aperture

→ it is possible to remap a dense grid of subapertures (redundant) into a sparse non-redundant array prior to Fizeau combination

Example: the Fiber Imager foR Single Telescope (FIRST) instrument concept

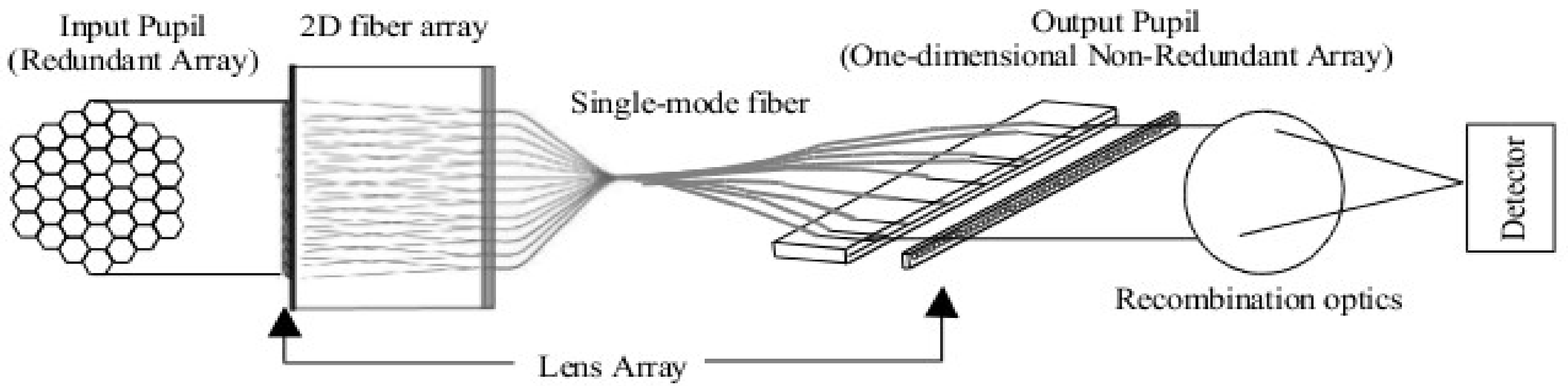

Fig.1. Schematic view of the insrtuemnts.

Remapping of a dense redundant array into a sparse non-redundant array
Single mode fibers used for spatial filtering

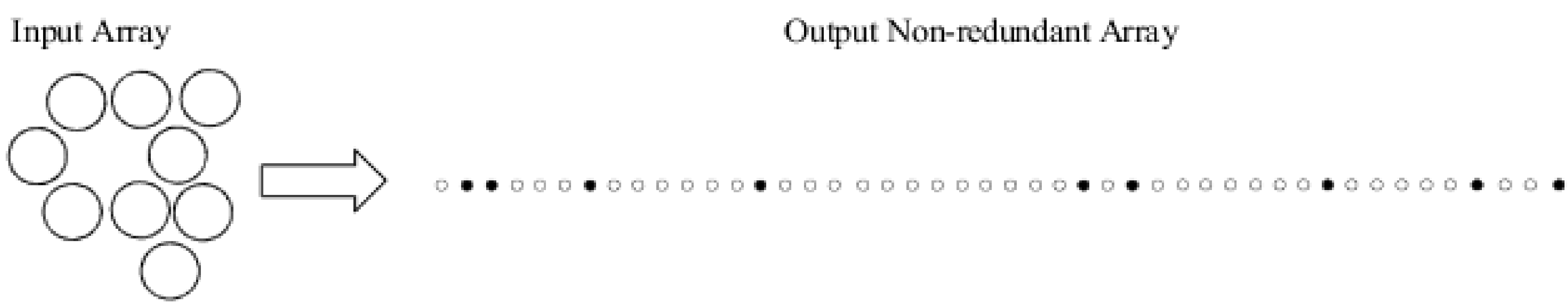

Kotani et al. 2008

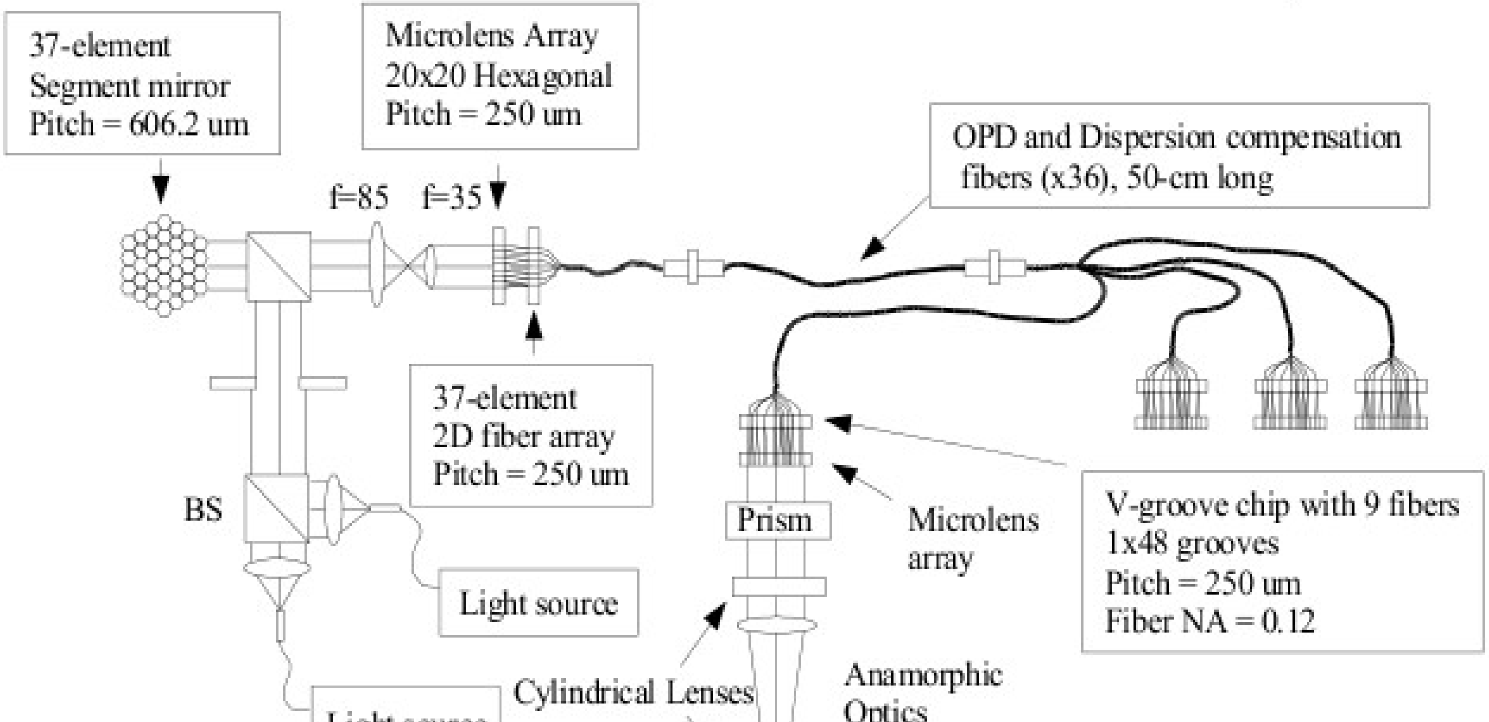
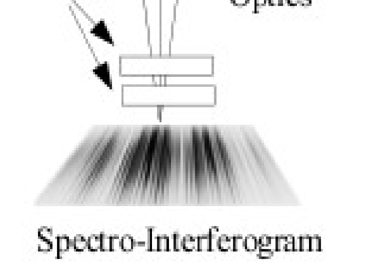

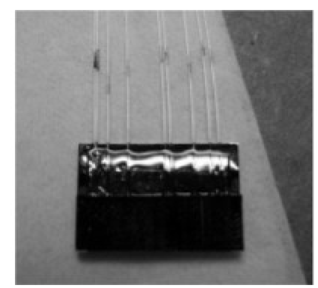

Fig.4. Left: 48 channel silicon v-groove chip from OZ optics. The fibers are arranged in non-redundantly. The fiber positions are [2,3,7,14,27,29,37,43,46]. Right: Laboratory obtained interferometric fringes using 9 fibers at a He-Ne laser.

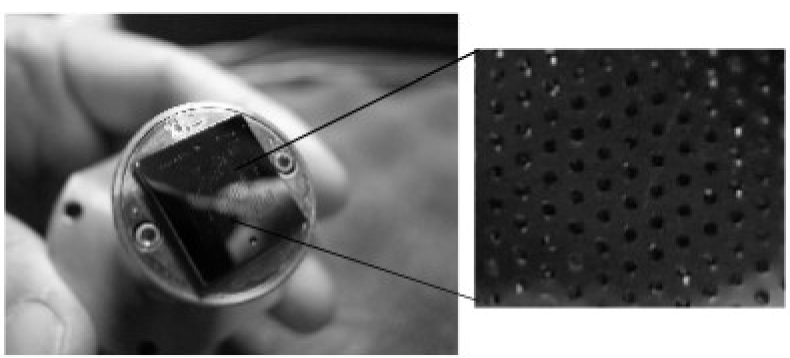

Fig.3. Left: 2D fiber array from FiberGuide Industries. The fiber pitch is 250 µm. Right: Segmented Deformable Mirror from IRIS AO. The pitch between adjacent segments is 606.2 µm including a 4 µm gap.

Kotani et al. 2008

Speckle imaging

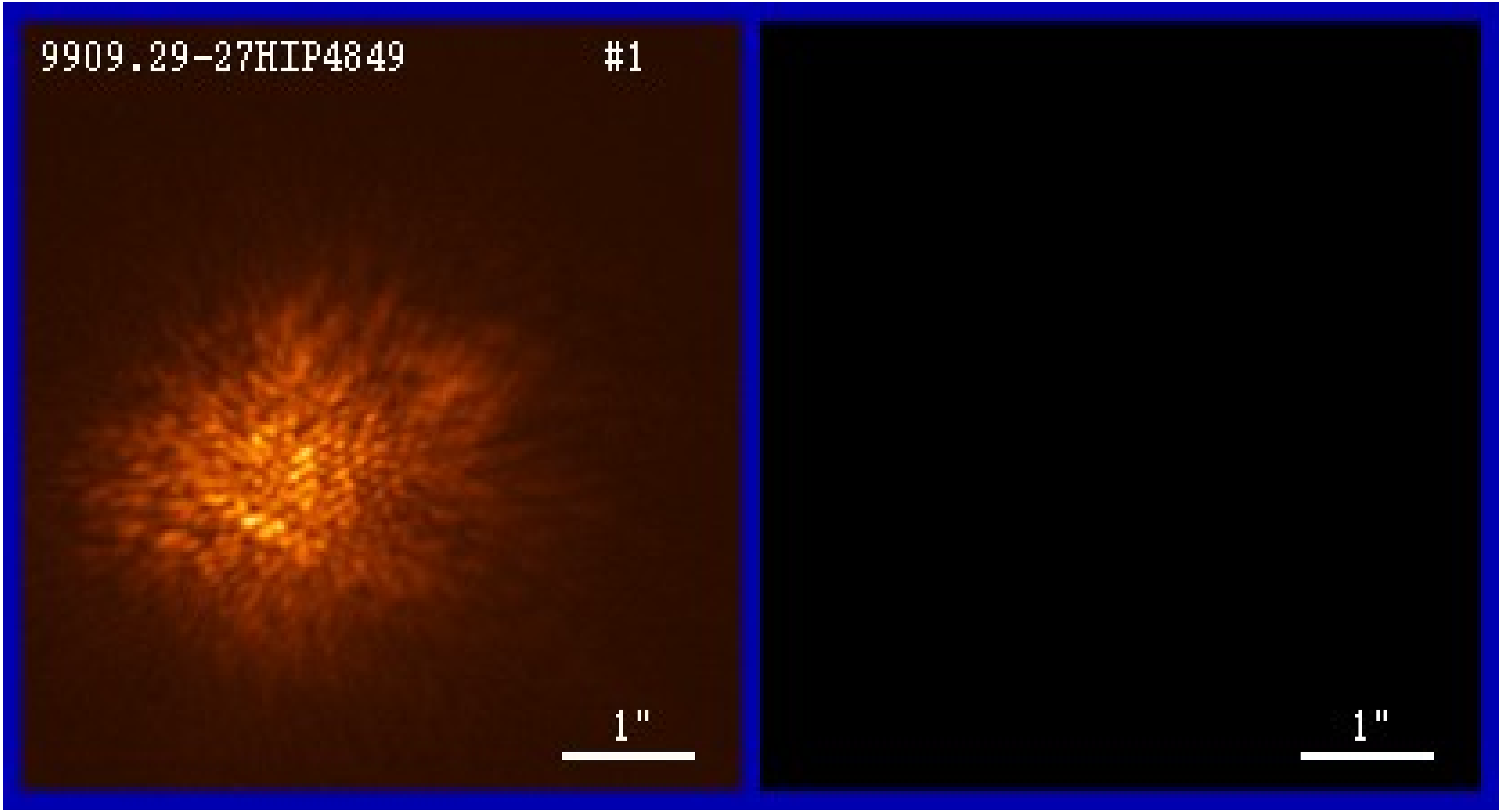

Real-time bispectrum speckle interferometry: 76 mas resolution.
Frame rate of data recording and processing: ~ 2 frames per second.
SAO 6 m telescope, K-band.

G. Weigelt, MPI for Radioastronomy, 1999

Speckle interferometry: reconstruction techniques

Single short exposure still contains signal at high spatial frequency.

Problem: phase and amplitude of the high spatial frequencies vary rapidly with time → long exposure will average high spatial frequencies to zero

Speckle interferometry (Power spectrum)
Solution developped by A. Labeyrie: average square modulus of images' Fourier transforms to obtain the square modulus FT of object

Problem: only amplitude of FT is recovered, not phase

Speckle interferometry (Bispectrum)
Solution developped by K Weigelt: average bispectrum (equivalent of phase closures in sparse interferometry) to also recover phase

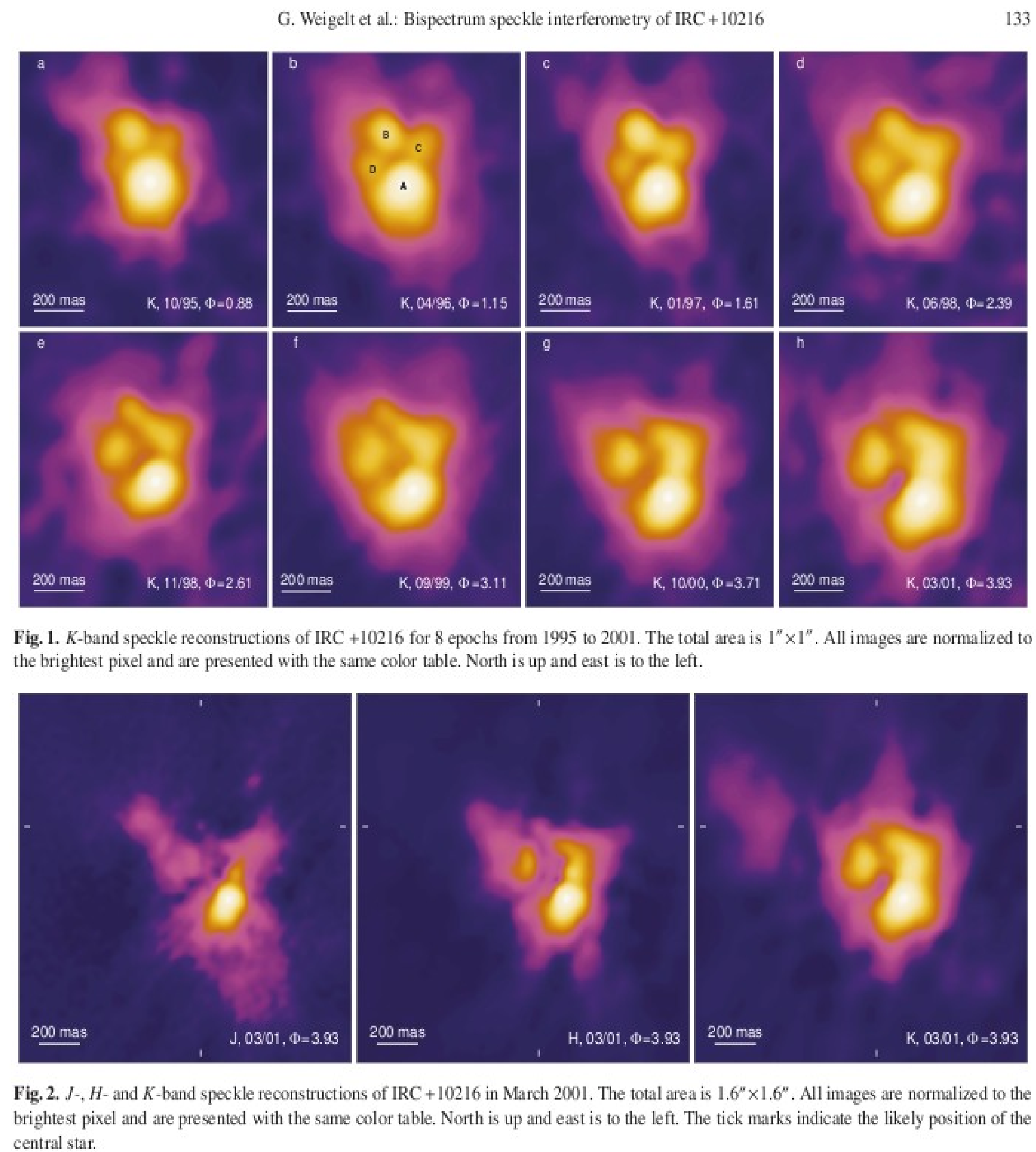
G. Weigelt et al.: Bispectrum speckle interferometry of IRC +10216 133

Fig. 1. *K*-band speckle reconstructions of IRC +10216 for 8 epochs from 1995 to 2001. The total area is 1″×1″. All images are normalized to the brightest pixel and are presented with the same color table. North is up and east is to the left.

Fig. 2. *J*-, *H*- and *K*-band speckle reconstructions of IRC +10216 in March 2001. The total area is 1.6″×1.6″. All images are normalized to the brightest pixel and are presented with the same color table. North is up and east is to the left. The tick marks indicate the likely position of the central star.

Speckle interferometry: reconstruction techniques

Object image : $f(x)$
Its Fourier transform: $F(u) = |F(u)| \exp[i\Phi(u)]$

Series of images (index n) is aquired. What is observed is the convolution of image and PSF:
$s_n(x) = f(x) \circ psf_n(x)$
In Fourier plane:
$S_n(u) = F(u) \times PSF_n(u)$

Power spectrum speckle interferometry (Labeyrie): measuring $|F(u)|$
$<|S(u)|^2> = |F(u)|^2 <|PSF(u)|^2>$

Speckle transfer function, calibrated on reference star

Bispectrum speckle interferometry (Weigelt):

Bispectrum : $F^3(u_1,u_2) = F(u_1)\ F(u_2)\ F(-u_1-u_2) = |F^3(u_1,u_2)| \exp[i\psi(u_1,u_2)]$

phase of object bispectrum

Average measured bispectrum:
$<|S^3(u_1,u_2)|> = F^3(u_1,u_2) <|H^3(u_1,u_2)|>$

bispectrum transfer function, has zero phase

Allows recovery of bispectrum phase: $\psi(u_1,u_2) = \Phi(u_1) + \Phi(u_2) - \Phi(u_1+u_2)$
(This is a closure phase measurement)